www.czasopisma.pan.pl PAN www.journals.pan.pl

ARCHIVES of FOUNDRY ENGINEERING

ISSN (2299-2944)
Volume 2023
Issue 4/2023

65 – 71

8/4

10.24425/afe.2023.146680

Published quarterly as the organ of the Foundry Commission of the Polish Academy of Sciences

Computed Tomography and Scanning Electron Microscopy Analysis of a Friction Stir Welded Al-Cu Joint

W.P. Depczyński *, D. Bańkowski, P.S. Młynarczyk
Radiography and Computed Tomography Laboratory, Department of Metal Science and Manufacturing Processes, Faculty of Mechatronics and Mechanical Engineering, Kielce University of Technology,
al. Tysiąclecia Państwa Polskiego 7, 25-314 Kielce, Poland
* Corresponding author. E-mail address: wdep@tu.kielce.pl

Received 02.03.2023; accepted in revised form 05.09.2023; available online 13.12.2023

Abstract

The study aimed touse3D computed tomography (CT) to analyse a joint between two dissimilar materials produced by friction stir welding (FSW). As the materials joined, i.e., aluminum and copper, differ in properties (e.g., density and melting point), the weld is predicted to have an inhomogeneous microstructure. The investigations involved applying microfocus computed tomography (micro-CT) to visualize and analyze the volumetric structure of the joint. Volume rendering is extremely useful because, unlike computer modelling, which requires many simplifications, it helps create highly accurate representations of objects. Image segmentation into regions was performed through global gray-scale thresholding. The analysis also included elemental mapping of the weld cross-sections using scanning electron microscopy (SEM) and examination of its surface morphology by means of optical microscopy (OP). The joint finds its use in developing elements used in the chemical, energetics and aerospace industries, due to the excellent possibilities of combining many different properties, and above all, reducing the weight of the structure.

Keywords: Friction stir welding, Non-destructive testing, Radiographic inspection, Computed tomography

1. Introduction

Joining dissimilar materials is critical in numerous applications, especially when there is a need for lower energy consumption, higher efficiency, and lighter weight [1]. Al-Cu joints are of particular importance in the electronics, transportation, and thermal power industries [2-4]. In traditional welding, large amounts of energy are required to generate heat so that the materials to be joined can be melted and fused. Friction stir welding is a solid-state joining technology that needs a lower heat input [1]. FSW is applied to butt weld metal sheets and plates. A special tool with a profiled pin, also called a probe, is required. It rotates while traversing forward along the contact line. This rotary motion generates friction heat, which is responsible first for heavy plastic deformation and then blending of the materials joined. The welding involves forging of the material at the rear of the tool [5].

The friction stir welding process is illustrated in Figure 1.

The weld is formed as a result of mechanical mixing of the materials in contact. To prevent discontinuities, such as entrapped oxide defects, it is recommended that the workpiece surfaces should be cleaned prior to FSW [7]. The resistance of the weld surface to oxidation can also be improved by properly designing the tool shoulder [8]. In friction stir welding, the mixing of the plastically deformed metals is due not only to an increase in their

temperature but also the formation of a stress field. The diffusion processes taking place in FSW lead to the friction blending of plastically deformed and displaced particles. The resulting weld has high strength properties [5], which are largely dependent on the microstructures of the base metals.

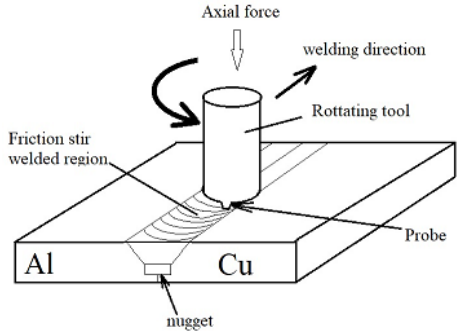

Fig. 1. A schematic diagram of the FSW process [6]

One of the key benefits of FSW is the fact that it is a solid-state joining process. No solidification shrinkage or hot cracking is observed. There is also no undesirable segregation of alloying elements or intermetallic phases as is the case with classical welding. The joint is assumed to have a dense non-porous structure. Another advantage of FSW, which makes it superior to traditional welding processes, is low energy consumption [9-12]. Although the economic and environmental factors are not of the utmost importance in the welding sector today, they may become relevant in the future.

Because of the occurrence of friction heat and plastic deformation induced by the rotation of the FSW tool, the following zones can be distinguished in a friction stir welded joint between two dissimilar metals: base metal 1 (BM1), base metal 2 (BM2), the heat affected zone (HAZ), the thermo-mechanically affected zone (TMAZ), and the stir zone (SZ), also known as the nugget zone (NZ) [2]. There are differences in material composition, microstructure, and properties between the zones, and all this will affect the weld quality, strength and efficiency [13-15].

Extensive research has been done to understand the FSW process, especially to determine the relationship between different welding parameters and the microstructure and mechanical properties of FSW joints [1, 16-26]. However, there has been hardly any qualitative analysis conducted along the whole length of an FSW joint. Generally, such joints are characterized on the basis of data obtained for several thin cross-sectional samples. Weld testing and analysis can be done using 3D computed tomography. This technique requires multiple measurements of X-ray attenuations, which are taken from different angles. The data are then processed to determine the quality and correctness (strength) of the weld. Radiography is suitable to assess not only the quality of welds but also castings and forgings [27]. Unlike surface and near-surface inspection methods (e.g., visual, liquid penetration, magnetic particle inspection) [28], X-ray testing provides information about the whole object. This volumetric analysis method is often used to test unconventionally machined products [29-33].

Multiple cross-sectional images produced by computed tomography are combined into one 3D model so that the whole object of interest or a selected “virtual slice” can be visualized [34-36]. Computed tomography uses radiation detectors to determine the object’s capacity to absorb radiation. This requires measuring the intensity of X-rays that have passed through the object [37]; obviously, it is lower than the initial one. It can be expressed as a function of radiation energy, material type and object thickness. The relationship can thus be written as:

$$I = \cdot I_0 e^{-\mu x} \tag{1}$$

where: I – the intensity of X-rays which have passed through a body,

I0 – the initial intensity of X-rays,

μ– the linear radiation absorption coefficient, characteristic of the material and X-ray wavelength,

x – the workpiece thickness.

X-ray radiation is created when accelerated electrons are suddenly stopped by matter. X rays are produced by two mechanisms: braking radiation and characteristic radiation [38]. Braking radiation is a result of the interaction of free electrons in the electric fields of the atomic nuclei and the electrons at the surface of matter decelerating the moving electrons. Accelerated electrons have enough energy to overcome Coulomb repulsion of electrons from the external orbits and get closer to the positively charged atomic nuclei, where they are scattered. Electrons scattered in this way lose their energy non-elastically while changing the travel directions and speeds [12]. The difference in the electron energy before and after deceleration is released in the form of photons of electromagnetic radiation – bremsstrahlung radiation [38]. A continuous spectrum is thus produced; all possible energy losses can be observed.

Characteristic X-rays are induced by a pass of an orbital electron from a higher energy level to a lower energy level, where an electron was earlier removed as a result of electron bombardment. Surplus electron energy is radiated in the form of a radiation quant characterized by a specific wavelength (K, L, M) [38]. The length of the emitted wave depends on the type of matter of the braking surface. The plots of the characteristic spectrum and that of the continuous bremsstrahlung spectrum define the relationship between the X-ray intensity and the wavelength.

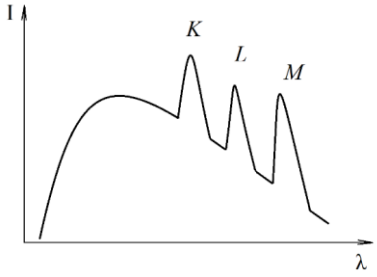

Fig. 2. X-ray intensity versus wavelength λ

The source of radiation in CT is an X-ray tube. The operating parameters, such as power and voltage, are selected according to the requirements. Unlike medical CT, industrial CT can be

employed to inspect materials with higher densities. Industrial testing of large metal (e.g., steel or aluminum) elements produced, for instance, by casting, metal forming or welding, requires high-energy radiation. Metals are tested with high-voltage X-ray tubes because of their high absorption capacity [27]. In industry, this method is being used on an increasing scale. CT is a common technique in defectoscopy (e.g., to check the internal structure of engineering materials), micromechanics (e.g., to inspect micromechanisms or precision components), geology (e.g., to determine the porosity of reservoir rocks, or to study fossils and minerals), archaeology (e.g., to visualize archaeological objects), and biology (e.g., to determine the structure of soft and hard biological tissues).

The aim of this study was to check if computed tomography would be suitable for analyzing the quality of a friction stir welded joint between two dissimilar materials with different properties (e.g., different densities). Volumetric analysis of such FSW joints, including the analysis of the formation of inter metallic compounds, is extremely interesting. The CT results were verified by scanning electron and optical microscopy, which provided information about the microstructure and chemical composition of the weld.

2. Materials and methods

The study focused on a friction stir welded joint between A1 aluminium and M1E copper. Both materials were in the form of 25 mm thick plates. As dissimilar materials, they have different chemical compositions and different properties. Aluminum, for example, is lighter and cheaper, while copper is a better heat and electricity conductor. The density of Al is 2.7g/cm3 whereas that of copper is 9.8g/cm3.Acorrding to Axon et al. [39] the lattice constant, for solid solution of Al is 0.4050nm. For a solid solution of Cu, the parameter is lower (a=0.363 nm), as determined by Pearson [40].

The joint was produced on a DMG DMU50 milling machine. The surfaces to be in contact were ground along the whole length before welding. The plates were clamped firmly in a vice and the friction stir welding was performed using a Ø32 mm HSS tool with a tapered pin at a speed of 900 rev/min, a feed of 30 mm/min, and a tool tilt angle of 0°. Then, the workpiece was mounted in an upside-down position so that the process could be repeated for the root side. The same parameters were used. When the joint was completed, a 55x55 mm sample was cut out for analysis.

The CT scanning and analysis were carried out at the Radiography and Computed Tomography Laboratory of the Kielce University of Technology, Poland, applying the world's first computed tomography system that combines three radiation sources, i.e., two micro- and one minifocus X-ray sources (225 kV, 450 kV, and 450 kV, respectively). The 450kV/450W microfocus X-ray source was selected for the tests. The examinations were conducted using a 440 kV and 232 µA (102.8 Wats of power) 450 kV X-ray tube with a 4 mm thick copper filter. A VAREX XRD 1611 detector was employed. The resolution of the detector is 4048 x 4048 pixels with a pixel size of 0.2 mm.

The scanning data were then processed and visualized using VG Studio 3.5.2. software. The images of the FSW Al-Cu joint were segmented using gray-scale thresholding [27]. The results were compared to the Al-Cu phase diagram.

The joint was then prepared for metallographic micro structural analysis by sectioning, mounting in cold setting resin (VariDur 10), and polishing first with a STRUERS automatic polisher and then by applying a 0.05 µm Al_2O_3 (microdiamond) suspension and colloidal silica. The preparation of the specimens for the OM and SEM examinations did not include etching. A JEOL JSM 7100F (field emission) scanning electron microscope was employed to study the weld structure, whereas an Oxford Instruments X-MAX EDS spectrometer was applied to determine its chemical composition.

3. Results and discussion

The heat generated during FSW is a result of the friction between the rotating tool and the materials joined, adhesion of the tool to these materials, and their plastic deformation around the tool. Figure 3 shows the macro-photograph of the FSW Al-Cu connection.

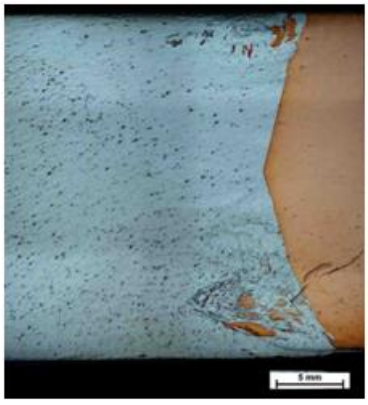

Fig. 3. Macrophotography of the FSW Al-Cu joint

The investigations aimed to visualize the volumetric structure of the joint by means of computed tomography - Figure 4to assess the mixing of the metals. The results were then compared with those obtained by SEM and OM.

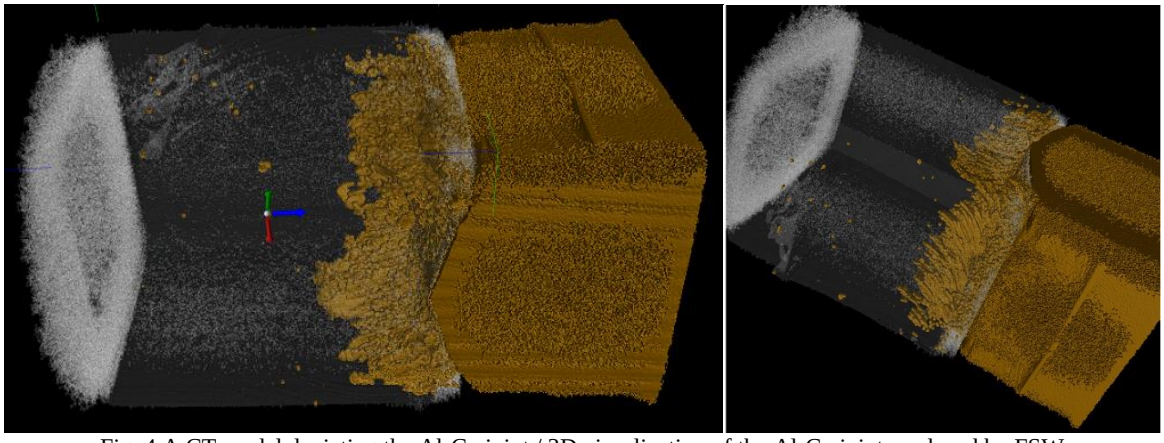

Fig. 4.A CT model depicting the Al-Cu joint / 3D visualization of the Al-Cu joint produced by FSW

The SEM analysis revealed local thermal changes and the accompanying diffusion of elements formed joints as a result of mixing materials. It was found that the heat produced by the rotating tool can lead to the transformation of the two metals into intermetallic compounds. Since the lattice constants, also called lattice parameters, of aluminum are much higher, the diffusion of copper in aluminum is easier than the opposite. Ionizing radiation analysis helped determine the amount and size of inclusions on both sides.

The Al-Cu phase diagram (Figure 5) can be used to predict the phases formed provided that the electron-matter interaction volume is smaller than the volume of the phase observed.

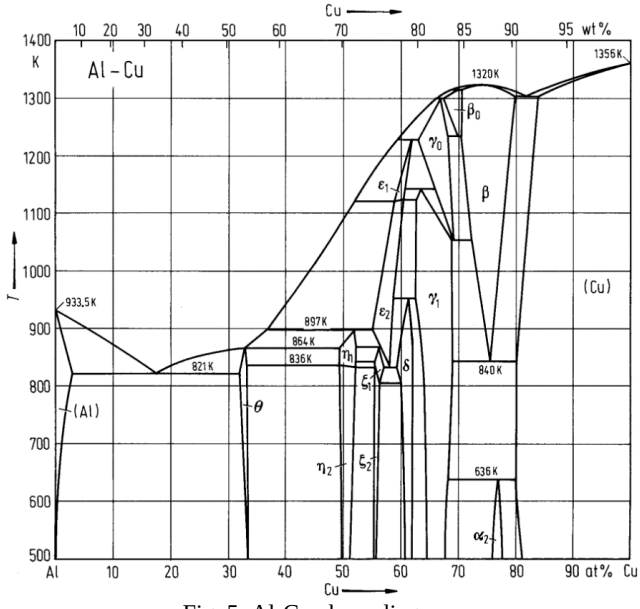

Fig. 5. Al-Cu phase diagram

The multiphase microstructure and the changes in the material flow at the Al-Cu interface were determined from the magnified images of the metallographic specimens - Figure 6.

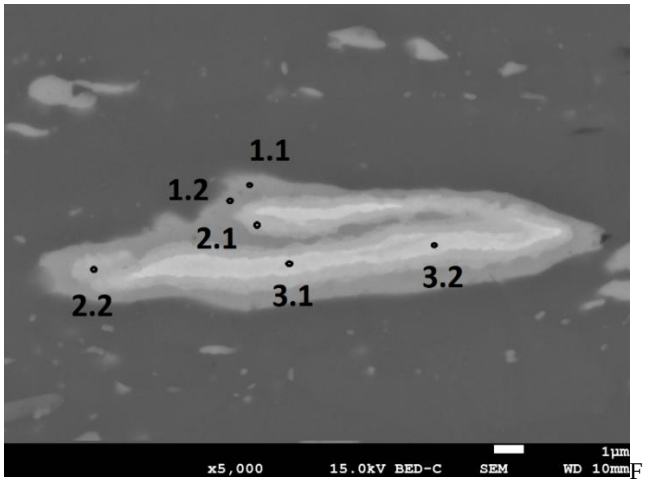

ig. 6. A SEM image of the Al-Cu joint

The compositions of the characteristic regions were determined by SEM-EDS. The results obtained for different points (Table 1) were compared with those of the phases in the Al-Cu phase diagram.

Table 1.
Results of the EDS analysis (in wt%) at the points marked in Figure 6

Point	Al	Si	Cu	Total
1.1	62.7	0.6	36.7	100
1.2	58.1	0.5	41.4	100
2.1	53.3	0.4	46.3	100
2.2	56.0	0.3	43.7	100
3.1	26.3	0.2	73.5	100
3.2	36.1	0.2	63.7	100

The SEM analysis of the Al-Cu junction area allows us to distinguish three different-looking areas, i.e., the first with an average content of about 60.4% Al and 39.0% Cu (points 1.1 and 1.2), the second on the aluminium side with an average content of about 54.6% Al and 45.0% Cu (points 2.1 and 2.2), and a third area with an average content of approximately 31.1% Al and

68.6% Cu (points 3.1 and 3.2). Silicon should be treated as an impurity. The workpieces of aluminium and copper probably contained trace amounts of silicon from the metallographic process (contamination with colloidal silica during polishing).

Figure 6 shows three different chemical composition observed at the interface between pure aluminum and pure copper. From the microphotographs, it is evident that no welding flaws (pores. voids. cracking. etc.) are present. The area adjacent to pure aluminum is 0,25÷0,8 μm in thickness; the average chemical composition at points 1.1 and 1.2 is 60.4% Al, 39.0% Cu and 0.6% Si, which suggests the presence of Al4Cu9 (δ). On the Cu side, there is an area with a thickness of about 0,5÷1 μm, where the average chemical composition is: 31.2% Al, 68.6% Cu, and 0.2% Si (points 3.1 and 3.2), which most probably is Al2Cu (θ).

From the Al-Cu phase diagram (Figure 5), it is apparent that locally the temperature may exceed 950 K. This temperature is close to the eutectoid temperature, at which Al4Cu9 (δ) forms. The intensity of friction heat generated during FSW is dependent on the tool type and the material thickness. If necessary, the weld microstructure can be modified. It is possible, for example, to reduce the formation of certain intermetallic phases by selecting the right process parameters.

Computer-based reconstruction of the area of interest required using VG Studio software, which helped determine the size, amount and distance from the joint line of copper inclusions in aluminum and of aluminum inclusions in copper. Graphic visualization provided information about the material in the stir zone, including the distribution of elements mixed due to friction heat and plastic deformation.

The heat affected zone (HAZ) is also visible on the image (Figure 7). It has a thickness of approx. 2.5 mm on the Cu-side and approx. 4 mm on the Al-side, where the material is denser and has greater thermal conductivity.

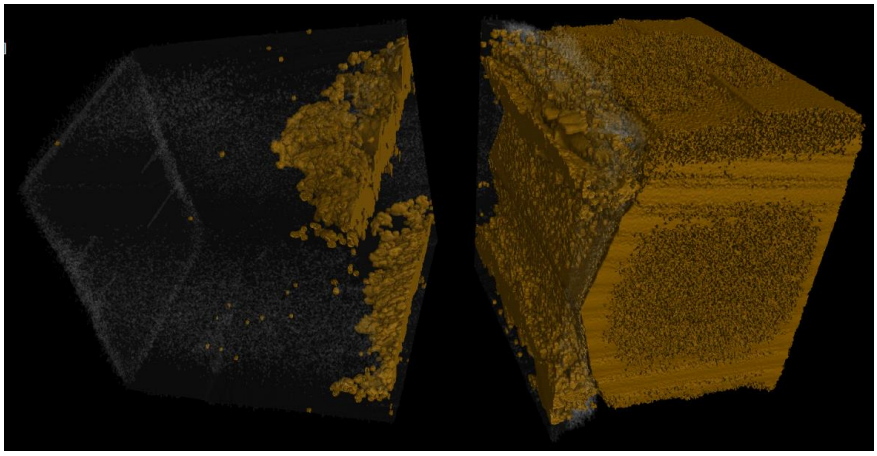

Fig. 7. The heat affected zone analyzed using VG Studio software

The type of materials used to create the joint using the FSW method and their properties - especially the melting point will be essential for the resulting joint. It may happen that the process parameters will be selected in such a way that the lower melting material will go into the liquid state, and the higher melting material will be solid. Figure 7 illustrates the plastically deformed plates joined together by FSW. The type of materials used (differences in the properties of copper and aluminium) affects the tendency to create material discontinuities. The main cause remains the high shrinkage during the solidification of aluminium. The amount of Cu particles on the Al side is lower than the amount of Al particles on the Cu side. On the Al side, there are only single inclusions of copper while on the Cu side, the area adjacent to Al has numerous agglomerates of Al. The occurrence of voids and pores in the weld (Figure 8) is directly dependent on the surface quality of the elements joined. If oxides are present at or near the workpiece surfaces, they should be removed because they may contaminate the weld and accordingly reduce its strength.

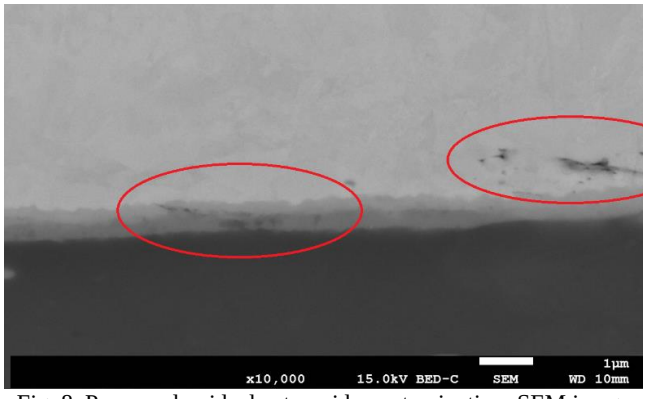

Fig. 8. Pores and voids due to oxide contamination, SEM image

4. Conclusions

From this study, it appears that Friction Stir Welding (FSW) can be an effective method of joining dissimilar materials and that computed tomography (CT) is well-suited to assess the quality of such joints.

The CT analysis confirmed that the two metals joined (Al and Cu) blended together throughout the whole volume of the weld.

Although the thermal changes accompanying the FSW process do not lead to the melting of the base metals, the increase in temperature is sufficient for the diffusion of atoms between the two metals and the formation of intermetallic phases.

References

[1] Zhao, Y., You, J., Qin, J., Dong, C., Liu, L., Liu, Z. & Miao, S. (2022). Stationary shoulder friction stir welding of Al–Cu dissimilar materials and its mechanism for improving the microstructures and mechanical properties of joint. *Materials Science & Engineering A* 837, 142754. https://doi.org/10.1016/j.msea.2022.142754.

[2] Zhou, L., Li, G.H., Zhang, R.X., Zhou, W.L., He, W.X., Huang, Y.X. & Song, X.G. (2019). Microstructure evolution and mechanical properties of friction stir spot welded dissimilar aluminum-copper joint. *Journal of Alloys and Compounds*. 775(15), 372-382. https://doi.org/10.1016/j.jallcom.2018.10.045.

[3] Tong, L., Xie, J.N., Liu, L., Chang, G. & Ojo, O.O. (2020). Microscopic appraisal and mechanical behavior of hybrid Cu/Al joints fabricated via friction stir spot welding-brazing and modified friction stir clinching-brazing. *Journal of Materials Research and Technology*. 9(6),13239-13249. https://doi.org/10.1016/j.jmrt.2020.09.042.

[4] Tian, W.H., Su, H. & Wu, C.S. (2020). Effect of ultrasonic vibration on thermal and material flow behavior, microstructure and mechanical properties of friction stir welded al/cu joints. *International Journal of Advanced Manufacturing Technology*. 107(1), 59-71. https://doi.org/10.1007/s00170-020-05019-0.

[5] Pilarczyk, J. (2005). *Engineer's Handbook 2, Welding*. Warszawa: Wydawnictwo Naukowo-Techniczne. (in Polish).

[6] Rajak, D.K., Pagar, D.D., Menezes, P.L. & Eyvazian, A. (2020). Friction-based welding processes: friction welding and friction stir welding. *Journal of Adhesion Science and Technology*. 34(24), 2613-2637. https://doi.org/10.1080/01694243.2020.1780716.

[7] Schneider, J., Chen, P. & Nunes, A.C. (2019). Entrapped oxide formation in the friction stir weld (FSW) process. *Metallurgical and Materials Transactions A*, 50, 257-270 https://doi.org/10.1007/s11661-018-4974-8.

[8] Rams, B., Pietras, A., & Mroczka K. (2014). Friction stir welding of elements made of cast aluminium alloys. *Archives of Foundry Engineering*. 59(1), 385-392.

[9] Martinsen, K., Hu, S.J. & Carlson, B.E. (2015). Joining of dissimilar materials. *CIRP Annals*. 64(2), 679-699. https://doi.org/10.1016/j.cirp.2015.05.006.

[10] Weman, K. (2011). *Welding processes handbook*. New York: Elsevier.

[11] Singh, R., Kumar, R., Feo, L., et al. (2016). Friction welding of dissimilar plastic/polymer materials with metal powder reinforcement for engineering applications. *Composites Part B: Engineering*. 101, 77-86. https://doi.org/10.1016/j.compositesb.2016.06.082.

[12] Rajak, D.K., Pagar, D.D., Menezes, P.L., et al. (2019). Fiber-reinforced polymer composites: manufacturing, properties, and applications. *Polymers*. 11(10), 1667. https://doi.org/10.3390/polym11101667.

[13] Lee, H.S., Lee, Y.R., Min, K.J. (2016). Effects of friction stir welding speed on AA2195 alloy. In: MATEC Web of Conferences. Vol. 45, France: EDP Sciences.

[14] Ramnath, B.V., Subramanian, S.A., Rakesh, R. et al. (2018). A review on friction stir welding of aluminium metal matrix composites. In IOP Conference Series: Materials Science and Engineering. 8-9 March 2018. IOP Publishing; 012103.

[15] Bankowski, D., Spadlo, S. (2017). Vibratory tumbling of elements made of Hardox400 steel. In 26th International Conference on Metallurgy and Materials (pp. 725-730).

[16] Karrar, G., Galloway, A., Toumpis, A., Li, H.J. & Al-Badouc, F. (2020). Microstructural characterisation and mechanical properties of dissimilar aa5083-copper joints produced by friction stir welding. *Journal of Materials Research and Technology*. 9(5), 11968-11979. https://doi.org/10.1016/j.jmrt.2020.08.073.

[17] Galvao, I., Loureiro, A. & Rodrigues, D.M. (2016). Critical review on friction stir welding of aluminium to copper. *Science and Technology of Welding and Joining*. 21(7), 523-546. https://doi.org/10.1080/13621718.2015.1118813.

[18] Ouyang, J., Yarrapareddy, E. & Kovacevic, R. (2006). Microstructural evolution in the friction stir welded 6061 aluminum alloy (T6-temper condition) to copper. *Journal of Materials Processing Technology*. 172(1), 110-122. https://doi.org/10.1016/j.jmatprotec.2005.09.013.

[19] Mehta, K.P. & Badheka, V.J. (2016). A review on dissimilar friction stir welding of copper to aluminum: process, properties, and variants. *Materials and Manufacturing Processes*. 31(3), 233-254. https://doi.org/10.1080/10426914.2015.1025971.

[20] Cao, F.J., Li, J.P., Hou, W.T., Shen, Y.F., Ni, R. (2021). Microstructural evolution and mechanical properties of the friction stir welded Al Cu dissimilar joint enhanced by post-weld heat treatment. *Materials Characterization.* 174, 110998. https://doi.org/10.1016/j.matchar.2021.110998.

[21] Hou, W.T., Shen, Z.K., Huda, N., Oheil, M., Shen, Y.F., Jahed, H. & Gerlich, A.P. (2021). Enhancing metallurgical and mechanical properties of friction stir butt welded joints of Al–Cu via cold sprayed Ni interlayer. *Materials Science and Engineering: A.* 809, 140992. https://doi.org/10.1016/j.msea.2021.140992.

[22] Mao, Y., Ni, Y., Qin, X.D.P. & Li, F. (2020). Microstructural characterization and mechanical properties of micro friction stir welded dissimilar al/cu ultra-thin sheets. *Journal of Manufacturing Processes.* 60, 356-365. https://doi.org/10.1016/j.jmapro.2020.10.064.

[23] Patel, N.P., Parlikar, P., Dhari, R.S., Mehta, K. & Pandya, M. (2019). Numerical modelling on cooling assisted friction stir welding of dissimilar Al-Cu joint. *Journal of Manufacturing Processes*. 47, 98-109. https://doi.org/10.1016/j.jmapro.2019.09.020.

[24] Mehta, K.P. & Badheka, V.J. (2017). Hybrid approaches of assisted heating and cooling for friction stir welding of copper to aluminum joints. *Journal of Materials Processing*

Technology. 239, 336-345. https://doi.org/10.1016/j.jmatprotec.2016.08.037.
[25] You, J.Q., Zhao, Y.Q., Dong, C.L., Wang, C.G., Miao, S., Yi, Y.Y. & Hai, Y.H. (2020). Microstructure characteristics and mechanical properties of stationary shoulder friction stir welded 2219-t6 aluminium alloy at high rotation speeds. *The International Journal of Advanced Manufacturing Technology*. 108, 987-996. https://doi.org/10.1007/s00170-019-04594-1.
[26] Li, D.X., Yang, X.Q., Cui, L., He, F.Z. & Zhang, X. (2015). Investigation of stationary shoulder friction stir welding of aluminum alloy 7075-t651. *Journal of Materials Processing Technology*. 222, 391-398. https://doi.org/10.1016/j.jmatprotec.2015.03.036.
[27] Depczynski, W., Spadlo, S., Mlynarczyk, P., Ziach, E., Hepner P. (2015). The selected properties of porous layers formed by pulse microwelding technique. In METAL 2015: 24TH International Conference on Metallurgy and Materials, 3 - 5 June 2015 (pp.1087-1092). Brno, Czech Republic.
[28] Bańkowski D. & Młynarczyk P. (2020). Visual testing of castings defects after vibratory machining. *Archives of Foundry Engineering*. 20(4), 72-76. DOI: 10.24425/afe.2020.133350.
[29] Mlynarczyk, P., Spadlo, S. (2016). The analysis of the effects formation iron - tungsten carbide layer on aluminum alloy by electrical discharge alloying process. In METAL 2016: 25th Anniversary International Conference on Metallurgy and Materials, 25 – 27 May 2016 (pp.1109-1114). Brno, Czech Republic.
[30] Depczynski, W. Jasionowski, R., Mlynarczyk, P. (2018). The impact of process variables on the connection parameters during pulse micro-welding of the H800 superalloy. In METAL 2018: 27TH International Conference on Metallurgy and Materials, 23 – 25 May 2018 (pp. 1506-1512). Brno, Czech Republic.
[31] Bankowski, D. & Spadlo, S. (2019). The use of abrasive waterjet cutting to remove flash from castings. *Archives of Foundry Engineering*. 19(3), 94-98. DOI: 10.24425/afe.2019.129617.
[32] Spadlo, S., Depczynski, W. & Mlynarczyk, P. (2017). Selected properties of high velocity oxy liquid fuel (HVOLF) - sprayed nanocrystalline WC-Co Infralloy(TM) S7412 coatings modified by high energy electric pulse. *Metalurgija*. 56(3-4), 412-414.
[33] Bonarski, J.T., Kania, B., Bolanowski, K. & Karolczuk, A. (2015). Utility of stress-texture characteristics of structural materials by X-ray. *Archives of Metallurgy and Materials*. 60(3), 2247-2252. DOI: 10.1515/amm-2015-0370.
[34] Jezierski, G. (1993). *Industrial radiography*. Warszawa: Wydawnictwa Naukowo-Techniczne. (in Polish).
[35] Cierniak, R. (2005). *Computed tomography. Construction of CT devices. Reconstruction algorithms*. Warszawa: Akademicka Oficyna Wydawnicza EXIT. (in Polish).
[36] Kielczyk, J. (2006). *Industrial radiography*. Wydawnictwo Gamma. (in Polish).
[37] Ratajczak, E. (2012). X-ray computed tomography (CT) for industrial tasks. *Pomiary Automatyka Robotyka*. 5, 104-113. (in Polish).
[38] Cullity, B.D. (1959). *Elements of X-Ray diffraction*. London: Addison-Wesley Publishing Company. Inc.
[39] Axon, H.J., Hume-Rothery, W. (1948). Proc. R. Soc. (London), Ser. A 193, 1.
[40] Pearson, W.B. (1958).: *ÑA Handbook of Lattice Spacings and Structures of Metals and Alloys*. Oxford: Pergamon Press.